

RSC Advances

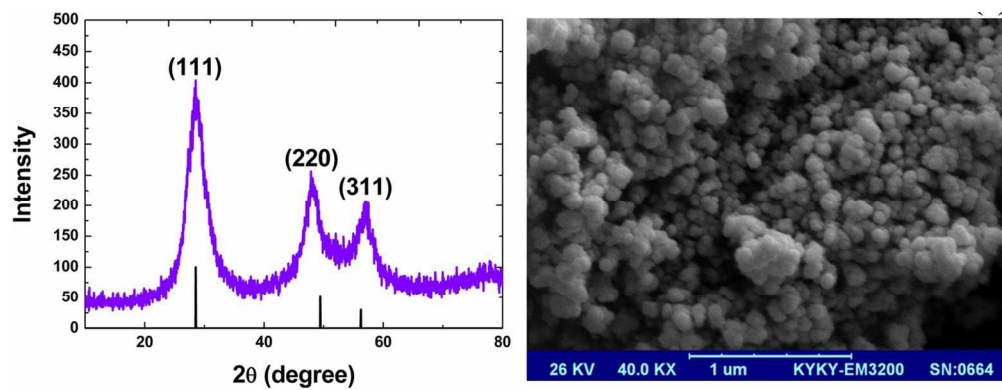


This is an *Accepted Manuscript*, which has been through the Royal Society of Chemistry peer review process and has been accepted for publication.

Accepted Manuscripts are published online shortly after acceptance, before technical editing, formatting and proof reading. Using this free service, authors can make their results available to the community, in citable form, before we publish the edited article. This *Accepted Manuscript* will be replaced by the edited, formatted and paginated article as soon as this is available.

You can find more information about *Accepted Manuscripts* in the [Information for Authors](#).

Please note that technical editing may introduce minor changes to the text and/or graphics, which may alter content. The journal's standard [Terms & Conditions](#) and the [Ethical guidelines](#) still apply. In no event shall the Royal Society of Chemistry be held responsible for any errors or omissions in this *Accepted Manuscript* or any consequences arising from the use of any information it contains.



246x93mm (150 x 150 DPI)

Optimization of the combined ultrasonic assisted/adsorption method for the removal of malachite green by Zinc sulfide nanoparticles loaded on activated carbon: Experimental design

M. Roosta*, M. Ghaedi, F. Yousefi

Chemistry Department, Yasouj University, Yasouj 75918-74831, Iran

Abstract

The present study was aimed to experimental design optimization applied to removal of malachite green (MG) from aqueous solution by ultrasound-assisted removal onto the Zinc sulfide nanoparticles loaded on activated carbon (ZnS-NP-AC). This nanomaterial was characterized using different techniques such as FESEM, BET, XRD and UV-Vis measurements. The effects of variables such as pH, initial dye concentration, adsorbent dosage (g) and sonication time on MG removal were studied using central composite design (CCD) and the optimum experimental conditions were found with desirability function (DF) combined response surface methodology (RSM). Fitting the experimental equilibrium data to various isotherm models show the suitability and applicability of the Langmuir model and the second-order equation model control the kinetic of the adsorption process. The small amount of proposed adsorbent (0.025 g) is applicable for successful removal of 22 mg L⁻¹ MG (>99%) in short time (5.0 min).

Keywords: Activated carbon; Adsorption; Experimental design; Zinc sulfide nanoparticles; Malachite green; Ultrasound-assisted.

* Author to whom correspondence should be addressed. Tel & fax: (0098)-74-33222048, E-mail: mostafaroosta.mr@gmail.com

1. Introduction

The dyes in industries effluents such as textile, leather, paper and plastics are of serious concern because of their adverse effects to human beings and environment [1, 2]. The dyes significant, importance and associated environmental problem come from their high visibility, undesirability and recalcitrance. Therefore, their removal from such industrial effluents is challenging requirement to produce a safe and clean environment [3].

Malachite green (MG) is classified as a basic dye consume in many industries (silk, wool, cotton, leather and paper) for coloring purposes, the structure is shown in Fig. 1. Furthermore, it is also employed as therapeutic agent to treat parasites, fungal and bacterial infections [4, 5]. Despite its extensive use, MG dye consists of toxic properties which are known to cause injuries to humans and animals by direct contact of inhalation and ingestion [6]. Therefore, the removal of MG from wastewater before discharging to the environment is necessary.

Many technologies have been developed for dye removal from industrial effluent including flocculation, coagulation, precipitation, biosorption, membrane filtration, electrochemical techniques and adsorption [7-10]. Among them, adsorption application follows a simple design, guarantees high efficiency and capacity, ease of operation, large scale ability with generable adsorbents [11–13]. Various materials such as activated carbon (AC), natural materials, polysaccharide materials, starch, bio adsorbents and agricultural wastes have been used for the removal of dyes from solution [14-17]. AC as non-toxic, low cost and easy available adsorbent has relatively high surface area, porous structure, total pore volume and large adsorption capacities. It is considered as a universal adsorbent for the removal of pollutants such as dyes from the wastewater with fast adsorption kinetics [18]. AC contain various reactive sites such OH, COOH, C=O and amide groups that in coincide to nanoparticle properties synergically improve the efficiency of adsorption based treatment procedure. In this technique application of

nano scale materials with high surface area enhance the removal percentage and adsorption capacity of AC based adsorbent. Nanoparticles possess distinguished properties such as high number of reactive atoms, high mechanical and thermal strength, high ordered structure and large number of vacant reactive surface sites in addition to metallic or semi-metallic behavior applied for removal of various toxic materials [19, 20].

Ultrasound irradiation is well known to accelerate chemical process due to the phenomenon of acoustic cavitation, that is, the formation, growth and collapse of micrometrical bubbles, formed by the propagation of a pressure wave through a liquid. Ultrasound, and its secondary effect, cavitation (nucleation, growth and transient collapse of tiny gas bubbles) improve the mass transfer through convection pathway that is emerged from physical phenomena such as micro-streaming, micro-turbulence, acoustic (or shock) waves and microjets without significant change in equilibrium characteristics of the adsorption/desorption system [21-23]. Shock waves have the potential of creating microscopic turbulence within interfacial films surrounding nearby solid particles. Acoustic streaming induced by the sonic wave is the movement of the liquid, which can be considered to be the conversion of sound to the kinetic energy [24]. Ultrasound has been proven to be a very useful tool in intensifying the mass transfer process and breaking the affinity between adsorbate and adsorbent [25, 26].

There are several experimental variables affecting the ultrasound-assisted removal of MG. A statistical design of experiment can be preferred to decrease the number of experiments and considered the interaction between variables [27, 28]. Designing and optimization of experiments and evaluation of the variables influence need to apply methods to be able for simultaneous optimization while consider the interaction of variables.

In the present work, ultrasound assisted as a simple, sensitive, inexpensive and rapid/assisted adsorption method followed by UV detection has been developed for removal of

MG. Influence of important variables (sonication time, pH, initial MG concentration and amount of adsorbent) were investigated and optimized by central composite design (CCD) combined with response surface methodology (RSM) using the desirability function (DF) as maximize criterion of the response. The results obtained from the presented models were compared with the experimental values.

The Zinc sulfide nanoparticles loaded AC (ZnS-NP-AC) was synthesis and subsequently characterized via different techniques such as field emission scanning electron microscopy (FESEM), transmission electron microscopy (TEM) and UV-Vis measurements. Then the adsorption kinetics and isotherms of MG removal on this adsorbent was investigated. The adsorption rates were evaluated by fitting the experimental data to conventional kinetic models such as pseudo first and second-order and intraparticle diffusion models. The proposed sorbent is useful for quantitative adsorption of the MG with high sorption capacities in short time.

2. Experimental

2.1. Instruments and Reagents

An ultrasonic bath with heating system (Tecno-GAZ SPA Ultra Sonic System, Italy) at 60 Hz of frequency and 130 W of power was used for the ultrasound-assisted adsorption procedure. The pH measurements were carried out using pH/Ion meter model-686 (Metrohm, Switzerland, Swiss) and the MG concentration was determined using Jusco UV-Vis spectrophotometer model V-530(Jasco, Japan) at a wavelength of 619 nm.

The morphology of the ZnS-NP-AC was observed by scanning electron microscopy (SEM; Hitachi S-4160, Japan) under an acceleration voltage of 15 kV. X-ray diffraction (XRD) pattern was recorded with an automated Philips X'Pert X-ray diffractometer with Cu K. radiation (40 kV and 30 mA) for 2 values over 10–80°. Absorption measurements were carried out on a

Perkin Elmer Lambda 25 spectrophotometer using a quartz cell with an optical path of 1 cm. The stock solution (200 mg L^{-1}) of MG was prepared by dissolving 100 mg of solid dye in 500 mL double distilled water and the working concentrations daily were prepared by its suitable dilution. A BET surface analyzer (Quantachrome NOVA 2000) was used to measure nitrogen adsorption-desorption isotherm at 77 K while before the measurement, the samples were degassed using helium at 553 K for 3 h.

All chemicals including malachite green, zinc acetate thioacetamide, activated carbon, NaOH, and HCl with the highest purity available were purchased from Merck Co. (Darmstadt, Germany).

2.2. Ultrasound assisted adsorption method

The removal of dye solutions were examined using ultrasound power combined with ZnS-NP-AC. The sonochemical adsorption experiment was carried out in a batch mode as follows: specified amounts of dye solution (50 mL) at known concentration (22 mg L^{-1}) and initial pH (6) with a known amount of adsorbent (0.025 g) were loaded into the flask and maintained the desired sonication time (5.0 min). At the end of the adsorption experiments, the sample was immediately centrifuged and analyzed.

2.3. Measurements of dye uptake

The dye concentrations were determined according to general photometry method at maximum wavelength (619 nm) over working concentration. The efficiency of MG removal was determined at different experimental condition according CCD method. The MG removal percentage was calculated using the following equation:

$$\% \text{ MG removal} = ((C_0 - C_t)/C_0) \times 100 \quad (1)$$

where C_0 (mg L^{-1}) and C_t (mg L^{-1}) is the concentration of target at initial and after time t respectively. The adsorbed MG amount (q_e (mgg^{-1})) was calculated by the following mass balance relationship:

$$q_e = (C_0 - C_e) V/W \quad (2)$$

Where C_0 and C_e (mg L^{-1}) are the initial and equilibrium dye concentrations in aqueous solution, respectively, V (L) is the volume of the solution and W (g) is the mass of the adsorbent.

2.4. Synthesis of zinc sulfide nanoparticle

The zinc sulfide nanoparticles (ZnS) were synthesized in an aqueous solution based on the reaction of zinc acetate ($\text{Zn}(\text{CH}_3\text{COO})_2$) with thioacetamide (CH_3CSNH_2) previously reported [29]. All reactions were carried out in oxygen free water under nitrogen. In a typical synthesis, 10 mL of freshly prepared thioacetamide solution (0.1 M) was added into another solution containing $\text{Zn}(\text{CH}_3\text{COO})_2$ and tri-sodium citrate ($\text{Na}_3\text{C}_6\text{H}_5\text{O}_7$) at a pH of 6.0 with vigorous stirring. The amounts of zinc acetate, thioacetamide, and tri-sodium citrate introduced were 0.5, 1, and 5 mmol, respectively, in a total volume of 50 mL. The resulting mixture was heated to 40 °C, and the growth of citrate - stabilized ZnS nanoparticles started gradually. After about 10 min, the solution turned milky white, which indicated the initial formation of ZnS nanoparticles. The mixture was maintained at 40 °C for 6 h and the color of the reaction solution became milky white mixed with light yellow. The ZnS nanoparticles obtained were separated from the reaction mixture by centrifugation, and washed several times with ultra - pure water and ethanol to remove the impurities and tri - sodium citrate. Finally, the ZnS nanoparticles were dried in a vacuum oven (ca. 0.1 MPa) for 6 h prior to being characterized.

For the preparation of ZnS-NP-AC, 500 mL of the dispersed ZnS nanoparticles suspension (0.5 g L^{-1}) was mixed with activated carbon (10 g) in a 1000 mL flask under magnetic stirring for up to 12 h, resulting in the deposition of the ZnS nanoparticles on the activated carbon. The carbon-supported ZnS nanoparticles were then filtered and extensively washed with double distilled water. The carbon-supported ZnS nanoparticles were generally dried at $110 \text{ }^\circ\text{C}$ in an oven for 10 h. A mortar was used to homogeneously ground the carbon-supported ZnS nanoparticles powders.

2.5. Central composite design

It is beneficial to evaluate and identify the most important variables with a minimum number of runs via an appropriate model. A five-level CCD was used to investigate the significance of the effects of parameters that designed by using the STATISTICA 7 (Table 1). The mathematical relationship between the four independent variables can be approximated by the second order polynomial model [30]:

$$y = \beta_0 + \sum_{i=1}^4 \beta_i x_i + \sum_{i=1}^4 \sum_{j=1}^4 \beta_{ij} x_i x_j + \sum_{i=1}^4 \beta_{ii} x_i^2 \quad (3)$$

where y is the predicted response (removal percentage); X_i 's are the independent variables (sonication time, pH, initial MG concentration and amount of adsorbent) that are known for each experimental run. The parameter β_0 is the model constant; β_i is the linear coefficient; β_{ii} are the quadratic coefficients and β_{ij} are the cross-product coefficients.

Response surface methodology (RSM) is a combination of mathematical and statistical techniques followed by optimal region determination allows the determination and evaluation of the relative significance of parameters, even in the presence of complex interactions [31]. The modeling is performed adjusting first or second order polynomials equations to the experimental

responses obtained in the experimental design, followed by a variance analysis (ANOVA) of the model. The validated model can be plotted in tridimensional graph, generating a surface response that corresponds to a response function used to determine the best operating conditions of a process.

2.6. Desirability function

Desirability function (DF) is a common and established technique to discover the global optimal conditions based on Derringer's desirability function [32, 33].

Each predicted response \hat{U}_i and experimental response U_i can be transformed to create a function for each individual response d_i and finally determine a global function D that should be maximized following selection of optimum value of affective variables with considering their interaction. Firstly, the response (U) is converted into a particular desirability function (df_i) in the range of 0 to 1. The $d_i=0$ represents completely undesirable response or minimum applicability and $d_i=1$ represents completely desirable or ideal response. The individual desirability scores d_i s are then combined using geometrical mean, on a single overall (global) desirability D , which is optimized to find the optimum set of input variables:

$$DF = [df_1^{v_1} \times df_2^{v_2} \dots \times df_n^{v_n}]^{1/n}, 0 \leq v_i \leq 1 \quad (i = 1, 2, \dots, n) \quad (4)$$

$$\sum_{i=1}^n v_i = 1$$

Where df_i indicate the desirability of the response U_i ($i = 1, 2, 3, \dots, n$) and v_i represents the importance of responses.

The individual desirability function for the i th characteristic is computed via following equation:

$$df_i = \left(\frac{U-\alpha}{\beta-\alpha}\right)^{w_i}, \alpha \leq U \leq \beta \quad (5)$$

$$df_i = 1, \quad U > \beta$$

$$df_i = 0, \quad U < \alpha$$

In Eq. (5), α and β are the lowest and highest obtained values of the response i and w_i is the weight.

3. Results and discussion

3.1. Characterization of adsorbent

Absorption spectra measurements for the prepared ZnS nanoparticles were conducted for 1 hr to 6 hrs interval and the variation of absorbance value with wavelength have been shown in Fig. 2a. The ZnS nanoparticles solution shows a well-resolved absorption maximum correspond to first electronic transition with a sufficiently narrow size distribution of ZnS nanoparticles. The shift of absorption peak to the shorter wavelengths show the decrease in size of the nanoparticles as a consequence of the quantum confinement. The figure shows that the citrate-stabilized ZnS nanoparticles have absorption edges in the range of 290-320 nm (4.26 - 3.86 eV). From the absorption spectra, energy band gap of ZnS nanoparticles was obtained using the following relation [34]:

$$(\alpha h\nu)^2 = A(E_g - h\nu) \quad (6)$$

Where E_g represents the nanoparticles band gap and A is a characteristic constant. A typical graph of $(\alpha h\nu)^2$ versus energy ($h\nu$) for ZnS nanoparticles was plotted. By extrapolation the linear portion of the respective curve to $(\alpha h\nu)^2 = 0$, the energy band gap was determined. The straight-line characteristic of the curve shows that the ZnS nanoparticles have the direct band gap in the range of 4.26 - 3.86 eV, while the bulk material has band gap of 3.67 eV.

Figure 2b shows the XRD pattern obtained from powdered ZnS nanoparticles synthesized at room temperature. The standard XRD pattern for ZnS (Joint Committee for Powder Diffraction Standards, JCPDS card No. 05-0566) is given at the bottom of Fig. 2b. The three broad peaks observed in the diffractogram at around 28.56° , 47.43° and 56.25° assigned to the planes (111), (220) and (311), respectively, show the cubic phase [35] of ZnS-NP-AC, while additional peaks correspond to ZnO or Zn(OH)₂ was not observed. The volume average hydrodynamic diameter for the ZnS nanoparticles (determined by laser light scattering) was found around 60 nm with narrow size distribution (Fig. 3a). The FESEM image of the ZnS nanoparticles (Fig. 3b) reveals that the ZnS nanoparticles are semi-cubical in shape and quite uniform in size distribution (in the range of 40–70 nm). The particle size was measured directly from this FESEM image agreed with respective approximate value determined by the laser light scattering.

Fig. 4 (a, b) shows the pore volume and pore area distribution curves of the ZnS-NP-AC based on the nitrogen equilibrium adsorption isotherm at 77 K. As can be seen, the adsorbent exhibit nearly narrow pore size distribution in the mesoporous domain. The BET surface area of ZnS-NP-AC was evaluated to be $1316 \text{ m}^2 \text{ g}^{-1}$. The measured total pore volume for ZnS-NP-AC was $0.658 \text{ cm}^3 \text{ g}^{-1}$ while the micropore volume was $0.197 \text{ cm}^3 \text{ g}^{-1}$. As can be seen from BET analysis, ZnS-NP-AC has porous structure and this evidence supports the enhancement of the surface area represents a good sorption capacity of such materials.

3.2. Central composite design (CCD)

As presented in Table 1, four independent variables (sonication time (X_1), pH (X_2), adsorbent dosage (X_3) and MG concentration (X_4)) were prescribed into three levels (low, basal and high) with coded value (-1, 0, +1) and the star points of +2 and -2 for $+\alpha$ and $-\alpha$ respectively were selected for each set of experiments and the levels of each factor are presented

in Table 1. 30 experiments for the optimization were performed according to the CCD and their responses are presented in Table 1. The main, interaction and quadratic effects were evaluated in this design. To find the most important effects and interactions, analysis of variance (ANOVA) was calculated using STATISTICA 7.0 (Table 2). A p-value less than 0.05 in the ANOVA table indicates the statistical significance of an effect at 95% confidence level. F-test was used to estimate the statistical significance of all terms in the polynomial equation within 95% confidence interval. Data analysis gave a semi-empirical expression of extraction recovery (ER %) with following equation:

$$y = 80.45 + 4.90x_1 + 2.01x_2 + 11.77x_3 - 7.11x_4 + 1.08x_1^2 - 1.08x_2^2 - 2.55x_3^2 - 0.92x_1x_3 + 2.87x_1x_4 + 1.44x_2x_4 - 2.28x_3x_4 \quad (7)$$

The plot of experimental values of removal (%) values versus those calculated from equation indicated a good fit, as presented in Fig. 5.

3.3. Response surface methodology

In the next step of the design, response surface methodology (RSM) was developed by considering all the significant interactions in the CCD to optimize the critical factors and describe the nature of the response surface in the experiment. Fig. 6 represents the relevant fitted response surfaces for the design and depicts the response surface plots of removal (%) versus significant variables. These plots were obtained for a given pair of factors at fixed and optimal values of other variables. The curvatures of these plots indicate the interaction between the variables.

For the adsorbent dosage, the response surfaces plots shown in Fig. 6 (a-c) demonstrated the changes in the percentage removal as a function of adsorbent dosage and other variables with interaction of them. The percentage removal increased with an increase in adsorbent dosage due to its high specific surface area and small particle size. At higher value probably due to increase

in surface area and availability of more active adsorption sites the rate of adsorption significantly increased. At lower amount of ZnS-NP-AC, the removal percentage because of high ratio of dye molecule to vacant site significantly decreased.

Fig. 6 (b, e, f) presents the interaction of pH with adsorption dosage, sonication time and initial MG concentration, respectively. The increased removal percentage of MG was observed with an increased in pH. This is probable due to the fact that at low initial pH, as a result of protonation of the functional groups, the ZnS-NP-AC surface get positively charged and the strong repulsive forces between the cationic dye molecules and adsorbent surface lead to significant decrease in the dye removal percentage. The increase in the initial pH lead to deprotonation of the active adsorption sites on the AC surface such as OH and COOH via electrostatic interaction and/or hydrogen bonding adsorbs the MG molecule.

As shown in Fig. 6 (a, d, e) it can be concluded that maximum adsorption of MG could be achieved when the sonication time was increased. The quick establishment of equilibrium and rapid adsorption show the efficiency of ultrasound power in terms of usage in wastewater treatment. The results showed that the initial adsorption rate is very rapid because of high available surface area and vacant site of adsorbent due to dispersion of adsorbent in to solution by ultrasonic power.

The effect of initial MG concentration on its removal percentage and the interaction of it by some factors were shown in Fig. 6 (c, d, f). It was seen that in despite of the increase in the amount of dye uptake, its removal efficiency was decreased and at lower dye concentrations, the ratio of solute concentrations to adsorbent sites is lower, which cause an increase in dye removal. At higher concentrations, lower adsorption yield is due to the saturation of adsorption sites. On the other hand, the percentage removal of dye was higher at lower initial dye concentrations and

smaller at higher initial concentrations, which clearly indicate that the adsorption of MG from its aqueous solution was dependent on its initial concentration.

3.4. Optimization of CCD by DF for extraction procedure

The profile for predicted values and desirability option in the STATISTICA 7.0 software is used for the optimization process (Fig. 7). Profiling the desirability of responses involves specifying the DF for each dependent variable (removal percentage) by assigning predicted values. The scale in the range of 0.0 (undesirable) to 1.0 (very desirable) is used to obtain a global function (D) that should be maximized according to efficient selection and optimization of designed variables. The CCD design matrix results (Table 1) show the maximum (99.63%) and minimum (44.45%) adsorption of MG. According to these values, DF settings for each dependent variable of removal percentage are depicted on the right hand side of Fig. 7: desirability of 1.0 was assigned for maximum removal (99.63%), 0.0 for minimum (44.45%) and 0.5 for middle (72.04%). On the left hand side of Fig. 7 (bottom) show the individual desirability scores are illustrated, to calculate the removal percentage. Since desirability 1.0 was selected as the target value, the overall response obtained from these plots with the current level of each variable in the model is depicted at the top (left) of Fig. 7. A view glance to figures shows that variable affect simultaneously the response and its desirability. On the basis of these calculations and desirability score of 1.0, maximum recovery (99.5 %) was obtained at optimum conditions set as: 5.0 min of sonication time, pH 6, 0.025 g of adsorbent and initial MG concentration of 22 mg L⁻¹. The validity of duplicate assenting experiments at the optimized value of all parameters was investigated. The results are closely co-related with the data obtained from desirability optimization analysis using CCD.

3.5. Adsorption equilibrium study

Generally, the equilibrium adsorption isotherm is used to give useful information about mechanism, properties and tendency of adsorbent toward each dye. The data obtained during equilibrium study has been fitted to various adsorption isotherm equations such as Langmuir, Freundlich, Temkin and Dubinin- Radushkevich (D-R) isotherms to discuss the equilibrium characteristics of the adsorption process [36–41]. The constant parameters and correlation coefficients (R^2) obtained from the plots of known equation equations for Langmuir, Freundlich, Tempkin and D–R are summarized in Table 3. Based on the linear form of Langmuir isotherm model [36] (according to Table 3), the values of K_L (the Langmuir adsorption constant ($L\ mg^{-1}$)) and Q_m (theoretical maximum adsorption capacity ($mg\ g^{-1}$)) were obtained from the intercept and slope of the plot of C_e/q_e vs C_e , respectively (Fig. 8a). The high correlation coefficient (0.9998) shows the applicability of Langmuir model for interpretation of the experimental data. The parameters of Freundlich isotherm model such as K_F ($(mg/g)/(mg/L)^{1/n}$) and n (the capacity and intensity of the adsorption) were calculated from the intercept and slope of the linear plot of $\ln q_e$ versus $\ln C_e$, respectively (Fig. 8b) and their values are presented in Table 3. The value of $1/n$ for Freundlich isotherm (0.237) show the high tendency of MG for the adsorption onto ZnS-NP-AC, while lower R^2 value (0.8496) show its unsuitability for fitting the experimental data.

The heat of the adsorption and the adsorbent–adsorbate interaction were evaluated by using Tempkin isotherm model [41]. B is the Tempkin constant related to heat of the adsorption ($J\ mol^{-1}$), T is the absolute temperature (K), R is the universal gas constant ($8.314\ J\ mol^{-1}\ K^{-1}$), K_T is the equilibrium binding constant ($L\ mg^{-1}$). The values of the Tempkin constants and the correlation coefficient are lower than the Langmuir value (Fig. 8c).

Another adsorption isotherm as D–R model was applied to estimate the porosity apparent free energy and the characteristic of adsorption. In the D–R isotherm K ($mol^2\ (kJ)^{-1}$) is a

constant related to the adsorption energy, Q_m (mg g^{-1}) is the theoretical saturation capacity, ϵ is the Polanyi potential. The slope of the plot of $\ln q_e$ versus ϵ^2 gives K and the intercept yields the Q_m value. The mean free energy of the adsorption (E), defined as the free energy change when one mole of ion is transferred from the solution to the surface of the sorbent, can be calculated. The value of correlation coefficient obtained from D–R model is lower than other isotherms values mentioned above (Fig. 8d). In this case, the D–R equation represents the poorer fit of the experimental data than the other isotherm equations. Among various isotherms model, the best usable model is Langmuir that due to charge of adsorbent and adsorbate hinder from multilayer adsorption.

3.6. Adsorption kinetic modeling

The experimental kinetic data of MG were correlated by such kinetic models including pseudo first and second-order, Elovich and intraparticle diffusion to study the rate and mechanism of an adsorption process. Table 4 summarized the properties of each model. The pseudo-first-order model (Lagergren model) [42] according to the equation listed in Table 4 by plotting the values of $\log (q_e - q_t)$ versus t may give a linear relationship that k_1 and q_e values can be determined from the slope and intercept of the obtained line, respectively (Fig. 9a).

The sorption kinetics may be described by a pseudo second-order model [43]. In despite of first order model, the plot of t/q_t versus t for the pseudo-second-order kinetic model gives a straight line with a high correlation coefficient that k_2 and equilibrium adsorption capacity (q_e) were calculated from the intercept and slope of this line, respectively (Fig. 9b). The values of R^2 and closeness of experimental and theoretical adsorption capacity (q_e) values show the applicability of the second order model to explain and interpret the experimental data (Table 4).

The R^2 value for pseudo-second-order kinetic model was found to be higher (0.999) and the calculated q_e value is mainly close to the experimental adsorption capacity value.

The later process possibility is explored using the intraparticle diffusion model based on diffusive mass transfer that adsorption rate expressed in terms of the square root of time (t) [44, 45]. The values of K_{diff} and C were calculated from the slope and intercept of the plot of q_t versus $t^{1/2}$ (Fig. 9c). C value is related to the thickness of the boundary layer and K_{diff} is the intraparticle diffusion rate constant ($\text{mg g}^{-1} \text{min}^{-1/2}$) were reported in Table 4. The values of K_{diff} and C were obtained from the final linear portion and their values are presented in Table 4. Since, the intraparticle curve did not pass through the origin; one can notice that in addition to the intraparticle diffusion model another stage such as pseudo-second order kinetic model act control the adsorption process.

3.7. Comparison with literature

The performance of the proposed method has been compared with other methods and some adsorbents (Table 5). The adsorption capacity and contact time for proposed method in comparison with all of the adsorbents are preferable and superior to the literature which shows satisfactory removal performance for MG [6, 46–49]. The ultrasonic-assisted enhancement of removal could be attributed to the high-speed microjets and high-pressure shock waves during the violent collapse of cavitation bubbles. The thoroughly mixing the adsorbent lead to significant reduce in mass transfer at similar conditions in the absence of ultrasonic. It was found that the removal percentage at the optimum conditions in the absence of ultrasonic was lower than 60% that significantly enhanced to the 99 % by using ultrasonic power.

4. Conclusion

In the present study, the analytical utility of experimental design for evaluation of optimum condition for the removal of MG in aqueous solution by ZnS-NP-AC coupled with ultrasound assisted adsorption method has been investigated. It was observed that the ZnS-NP-AC is an efficient adsorbent for the removal of MG. The combination of ultrasonic power in addition to application of ZnS-NP-AC is an efficient, fast and sensitive adsorption method for the removal of MG. The influences of experimental parameters on the removal percentage were investigated using CCD combined with RSM. Fitting the experimental equilibrium data show the suitability and applicability of the Langmuir model with the second-order equation model to control the kinetic of the adsorption process. The optimum operating variables (0.025 g adsorbent, 5.0 min contact time, pH 6 and 22 mg L⁻¹ MG) to obtain maximum MG removal (>99%) were determined by DF. The advantage of method is possibility to use nontoxic adsorbent for removal of large amount of MG in short time via a simple procedure. The developed procedure provided many advantages such as high percentage removal, simplicity, stability and easy to operate.

Acknowledgement

The authors express their appreciation to the Graduate School and Research Council of the University of Yasouj for financial support of this work. The author acknowledges financial support from the Iran National Science Foundation (INSF-No: 92039361).

References

- [1] C. Pradeep Sekhar, S. Kalidhasan, V. Rajesh, N. Rajesh, *Chemosphere* 77 (2009) 842–847.
- [2] W.H. Li, Q.Y. Yue, B.Y. Gao, Z.H. Ma, Y.J. Li, H.X. Zhao, *Chem. Eng. J.* 171 (2011) 320–327.
- [3] G. Mezohegyi, F.P. van der Zee, J. Font, A. Fortuny, A. Fabregat, *J. Environ. Manage.* 102 (2012) 148–164.
- [4] M.A. Ahmad, R. Alrozi, *Chem. Eng. J.* 171 (2011) 510–516.
- [5] L. Ai, H. Huang, Z. Chen, X. Wei, J. Jiang, *Chem. Eng. J.* 156 (2010) 243–249.
- [6] M.H. Baek, C.O. Ijagbemi, Se-Jin O, D.S. Kim, *J. Hazard. Mater.* 176 (2010) 820–828.
- [7] B.Y. Shi, G.H. Li, D.S. Wang, C.H. Feng, H.X. Tang, *J. Hazard. Mater.* 143 (2007) 567–574.
- [8] F. Delval, G. Crini, N. Morin, J. Vebrel, S. Bertini, G. Torri, *Dyes Pigm.* 53 (2002) 79–92.
- [9] K.V. Kumar, *J. Hazard. Mater.* 136 (2006) 197–202.
- [10] M. Ghaedi, H. Khajehsharifi, A. Hemmati Yadkuri, M. Roosta, A. Asghari, *Toxicol. Environ. Chem.* 94 (2012) 873–883.
- [11] M. Roosta, M. Ghaedi, A. Asfaram, *RSC Adv.* 5 (2015) 57021–57029.
- [12] D.K. Kweon, J.K. Choi, E.K. Kim, S.T. Lim, *Carbohydr. Polym.* 46 (2001) 171–177.
- [13] M. Roosta, M. Ghaedi, A. Daneshfar, S. Darafarin, R. Sahraei, M.K. Purkait, *Ultrason. Sonochem.* 21 (2014) 1441–1450.
- [14] F. Delval, G. Crini, J. Vebrel, M. Knorr, G. Sauvin, E. Conte, *Macromol. Symp.* 203 (2003) 165–171.

- [15] F. Delval, G. Crini, L. Janus, J. Vebrel, M. Morcellet, *Macromol. Symp.* 166 (2001) 103–108.
- [16] T. Santhi, S. Manonmani, *Sustain. Environ. Res.* 22 (2012) 45–51.
- [17] G. Crini, *Bioresour. Technol.* 97 (2006) 1061–1085.
- [18] P. Sathishkumar, M. Arulkumar, T. Palvannan, *J. Clean. Prod.* 22 (2012) 67–75.
- [19] M. Ghaedi, S. Heidarpour, S. Nasiri Kokhdan, R. Sahraie, A. Daneshfar, B. Brazesh, *Powder Technol.* 228 (2012) 18–25.
- [20] M. Ghaedi, K. Niknam, S. Zamani, H. Abasi Larki, M. Roosta, M. Soylak, *Material Science and Engineering C* 33 (2013) 3180–3189.
- [21] G.L. Maddikeri, A.B. Pandit, P.R. Gogate, *Ind. Eng. Chem. Res.* 51 (2012) 6869–6876.
- [22] B.R. Reddy, T. Sivasankar, M. Sivakumar, V.S. Moholkar, *Ultrason. Sonochem.* 17 (2010) 416–426.
- [23] M. Roosta, M. Ghaedi, A. Daneshfar, R. Sahraei, A. Asghari, *Ultrason. Sonochem.* 21 (2014) 242–252.
- [24] L.H. Thompson, L.K. Doraiswamy, *Ind. Eng. Chem. Res.* 38 (1999) 1215–1249.
- [25] J.P.S. Fernandes, B.S. Carvalho, C.V. Luchez, M.J. Politi, C.A. Brandt, *Ultrason. Sonochem.* 18 (2011) 489–493.
- [26] M. Roosta, M. Ghaedi, A. Daneshfar, *Food Chem.* 161 (2014) 120–126.
- [27] E.A. Diler, R. Ipek, *Mater. Sci. Eng., A* 548 (2012) 43–55.
- [28] F. Momenbeik, M. Roosta, A.A. Nikoukar, *J. Chromatogr. A* 1217 (2010) 3770–3773.
- [29] M. Ghaedi, H.A. Larki, S.N. Kokhdan, F. Marahel, R. Sahraei, A. Daneshfar, M.K. Purkait, *Environ. Prog. Sustainable Energy* 32 (2013) 535–542.
- [30] M.B. Hossain, N.P. Brunton, A. Patras, B. Tiwari, C.P.O. Donnell, A.B. Martin-Diana, C.B. Ryan, *Ultrason. Sonochem.* 19 (2012) 582–590.

- [31] M. Roosta, M. Ghaedi, M. Mohammadi, *Powder Technol.* 267 (2014) 134–144.
- [32] G. Derringer, R. Suich, *J. Qual. Technol.* 12 (1980) 214–219.
- [33] A. Malenovic, Y. Dotsikas, M. Maskovic, B. Jancic–Stojanovic, D. Ivanovic, M. Medenica, *Microchem. J.* 99 (2011) 454–460.
- [34] Y.S. Ho, *J. Coll. Inter. Sci.* 333 (2009) 412.
- [35] A. Goudarzi, G. Motedayen Aval, S.S. Park, M.C. Choi, R. Sahraei, M. Habib Ullah, A. Avane, C.S. Ha, *Chem. Mater.* 21, (2009) 2375–2385.
- [36] M. Ghaedi, H. Khajesharifi, A. Hemmati Yadkuri, M. Roosta, R. Sahraei, A. Daneshfar, *Spectrochim. Acta, Part A* 86 (2012) 62–68.
- [37] I. Langmuir, *J. Am. Chem. Soc.* 38 (1916) 2221–2295.
- [38] H.M.F. Freundlich, *J. Phys. Chem.* 57 (1906) 385–471.
- [39] C. Ng, J.N. Losso, W.E. Marshall, R.M. Rao, *Bioresour. Technol.* 85 (2002) 131–135.
- [40] L. Aia, C. Zhang, Z. Chen, *J. Hazard. Mater.* 192 (2011) 1515–1524.
- [41] M.J. Temkin, V. Pyzhev, *Acta Physiochim.USSR* 12 (1940) 217–222.
- [42] S. Lagergren, *Handlingar* 24 (1898) 1–39.
- [43] D.M. Ruthven, K.F. Loughlin, *Chem. Eng. Sci.* 26 (1971) 577–584.
- [44] J.J. Pignatello, F.J. Ferrandino, L.Q. Huangm, *Environ. Sci. Technol.* 27 (1993) 1563–1571.
- [45] D. Ozdes, C. Duran, H.B. Senturk, *J. Environ. Manag.* 92 (2011) 3082–3090.
- [46] R.R. Kannan, M. Rajasimman, N. Rajamohan, B. Sivaprakash, *Int. J. Environ. Res.* 4 (2010) 817–824.
- [47] T. Santhi, S. Manonmani, T. Smitha, *J. Hazard. Mater.* 179 (2010) 178–186.
- [48] H. Zhang, Y. Tang, X. Liu, Z. Ke, X. Su, D. Cai, X. Wang, Y. Liu, Q. Huang, Z. Yu, *Desalination* 274 (2011) 97–104.

- [49] R.P. Han, Y. Wang, Q. Sun, L.L. Wang, J.Y. Song, X.T. He, C.C. Dou, J. Hazard. Mater. 175 (2010) 1056–1061.

Figure captions:

Fig. 1. Chemical structure of MG.

Fig. 2. (A) Variation of absorption spectra of the ZnS nanoparticles at different time interval and **(B)** X-ray diffraction (XRD) pattern of the citrate-stabilized ZnS nanoparticles.

Fig. 3. (a) Histogram of the ZnS nanoparticles size distribution and **(b)** FESEM image of the ZnS nanoparticles.

Fig. 4. Pore size distribution curves of the ZnS-NP-AC.

Fig. 5. The experimental data versus the predicted data of normalized removal of MG.

Fig. 6. Response surfaces for the CCD: **(a)** Adsorbent dosage–Sonication time; **(b)** Adsorbent dosage–pH; **(c)** Adsorbent dosage–MG concentration; **(d)** Sonication time–MG concentration; **(e)** pH–Sonication time and **(f)** pH–MG concentration.

Fig. 7. Profiles for predicated values and desirability function for removal percentage of MG. Dashed line indicated current values after optimization.

Fig. 8. Plot of equilibrium isotherms for the adsorption of MG dye onto ZnS-NP-AC: **(a)** Langmuir; **(b)** Freundlich; **(c)** Temkin and **(d)** Dubinin–Radushkevich isotherms.

Fig. 9. Kinetic plots for the adsorption of MG dye onto ZnS-NP-AC: **(a)** Pseudo-first-order kinetic; **(b)** Pseudo-second-order kinetic and **(c)** intraparticle diffusion model.

Table 1. Experimental factors and levels in the central composite design.

Factors	Levels				
	Low (-1)	Central (0)	High (+1)	- α	+ α
(X ₁) Sonication time (min)	2.0	3.5	5.0	0.5	6.5
(X ₂) pH	4	5.5	7	2.5	8.5
(X ₃) Adsorbent dosage (g)	0.010	0.016	0.022	0.004	0.028
(X ₄) MG concentration (mg L ⁻¹)	15	25	35	5	45

Runs	X ₁	X ₂	X ₃	X ₄	Removal (%)
1	2	4	0.010	35	49.59
2	2	4	0.022	15	96.66
3	2	7	0.010	15	68.52
4	2	7	0.022	35	75.61
5	5	4	0.010	15	75.55
6	5	4	0.022	35	85.20
7	5	7	0.010	35	73.98
8	5	7	0.022	15	99.63
9 (C)	3.5	5.5	0.016	25	82.04
10 (C)	3.5	5.5	0.016	25	80.44
11	2	4	0.010	15	68.52
12	2	4	0.022	35	70.73
13	2	7	0.010	35	57.72
14	2	7	0.022	15	97.52
15	5	4	0.010	35	68.29
16	5	4	0.022	15	99.18
17	5	7	0.010	15	73.33
18	5	7	0.022	35	88.58
19 (C)	3.5	5.5	0.016	25	78.88
20 (C)	3.5	5.5	0.016	25	80.88
21	0.5	5.5	0.016	25	75.55
22	6.5	5.5	0.016	25	94.88
23	3.5	2.5	0.016	25	69.77
24	3.5	8.5	0.016	25	83.33
25	3.5	5.5	0.004	25	44.44
26	3.5	5.5	0.028	25	96.88
27	3.5	5.5	0.016	5	97.70
28	3.5	5.5	0.016	45	66.93
29 (C)	3.5	5.5	0.016	25	79.33
30 (C)	3.5	5.5	0.016	25	81.11

Table 2. Analysis of variance (ANOVA) for CCD.

Source of variation	Sum of square	Degree of freedom	Mean square	F- value	P- value
X_1	575.796	1	575.796	419.923	0.000005
X_1^2	32.250	1	32.250	23.520	0.004675
X_2	97.069	1	97.069	70.792	0.000389
X_2^2	32.131	1	32.131	23.433	0.004712
X_3	3325.250	1	3325.250	2425.077	0.000000
X_3^2	178.992	1	178.992	130.538	0.000090
X_4	1214.704	1	1214.704	885.874	0.000001
X_4^2	3.512	1	3.512	2.561	0.170415
X_1X_2	2.693	1	2.693	1.964	0.219977
X_1X_3	13.569	1	13.569	9.896	0.025501
X_1X_4	131.819	1	131.819	96.135	0.000188
X_2X_3	0.261	1	0.261	0.190	0.680980
X_2X_4	33.083	1	33.083	24.127	0.004428
X_3X_4	83.437	1	83.437	60.850	0.000555
Lack of Fit	56.436	10	5.644	4.116	0.065902
Pure Error	6.856	5	1.371		
Total SS	5813.592	29			

Table 3. Isotherm constant parameters and correlation coefficients calculated for the adsorption of MG onto 0.025 g of ZnS-NP-AC.

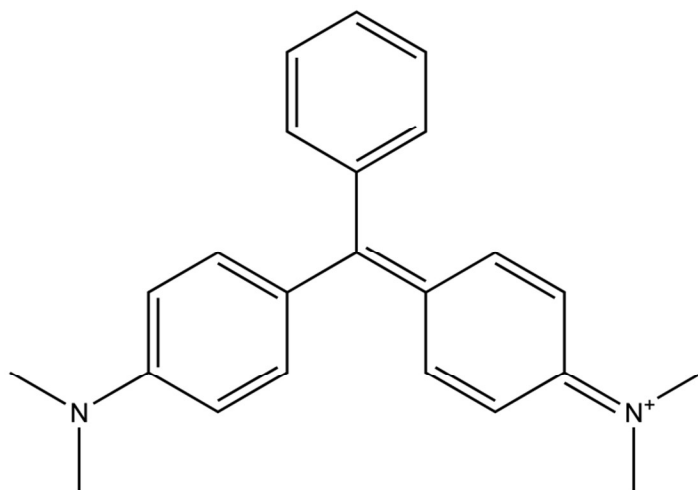
Isotherm	Equation	parameters	Value of parameters
Langmuir	$C_e/q_e = 1/(K_a Q_m) + C_e/Q_m$	Q_m (mg g ⁻¹)	51.55
		K_a (L mg ⁻¹)	12.12
		R^2	0.9998
Freundlich	$\ln q_e = \ln K_F + (1/n) \ln C_e$	$1/n$	0.237
		K_F (L mg ⁻¹)	37.02
		R^2	0.8496
Tempkin	$q_e = B_1 \ln K_T + B_1 \ln C_e$	B_1	5.499
		K_T (L mg ⁻¹)	1478.37
		R^2	0.929
Dubinin and Radushkevich (D-R)	$\ln q_e = \ln Q_s - B\varepsilon^2$	Q_s (mg g ⁻¹)	40.90
		B (mol ² (kJ ²) ⁻¹)	8E-9
		R^2	0.8812

Table 4. Kinetic parameters for the adsorption of MG onto ZnS-NP-AC.

Model	Equation	Parameters	Value of parameters
First-order kinetic	$\text{Log}(q_e - q_t) = \log(q_e) - (k_1/2.303)t$	k_1	0.6347
		q_e (calc)	15.696
		R^2	0.9818
Second-order kinetic	$(t/q_t) = 1/(k_2 q_e^2) + 1/q_e(t)$	k_2	0.162
		q_e (calc)	43.859
		R^2	0.9990
Intraparticle diffusion	$q_t = K_{\text{dif}} t^{1/2} + C$	K_{dif}	7.452
		C	27.599
		R^2	0.9229
		q_e (exp)	43.734

Table 5. Comparison for the removal of dyes by different methods and adsorbents.

Adsorbent	Adsorbate	Adsorption capacity (mg g ⁻¹)	Concentration (mg L ⁻¹)	Contact time (min)	Ref
Raw coffee beans	MG	55.3	50	30	[7]
Hydrilla verticillata biomass	MG	69.88	200	150	[46]
Ricinus communis	MG	27.78	50	90	[47]
Brown-rotted pine wood	MG	42.43	7.0	>600	[48]
Zeolite	MG	23.90	50	240	[49]
ZnS-NP-AC	MG	51.55	22	5.0	This work

**Fig. 1**

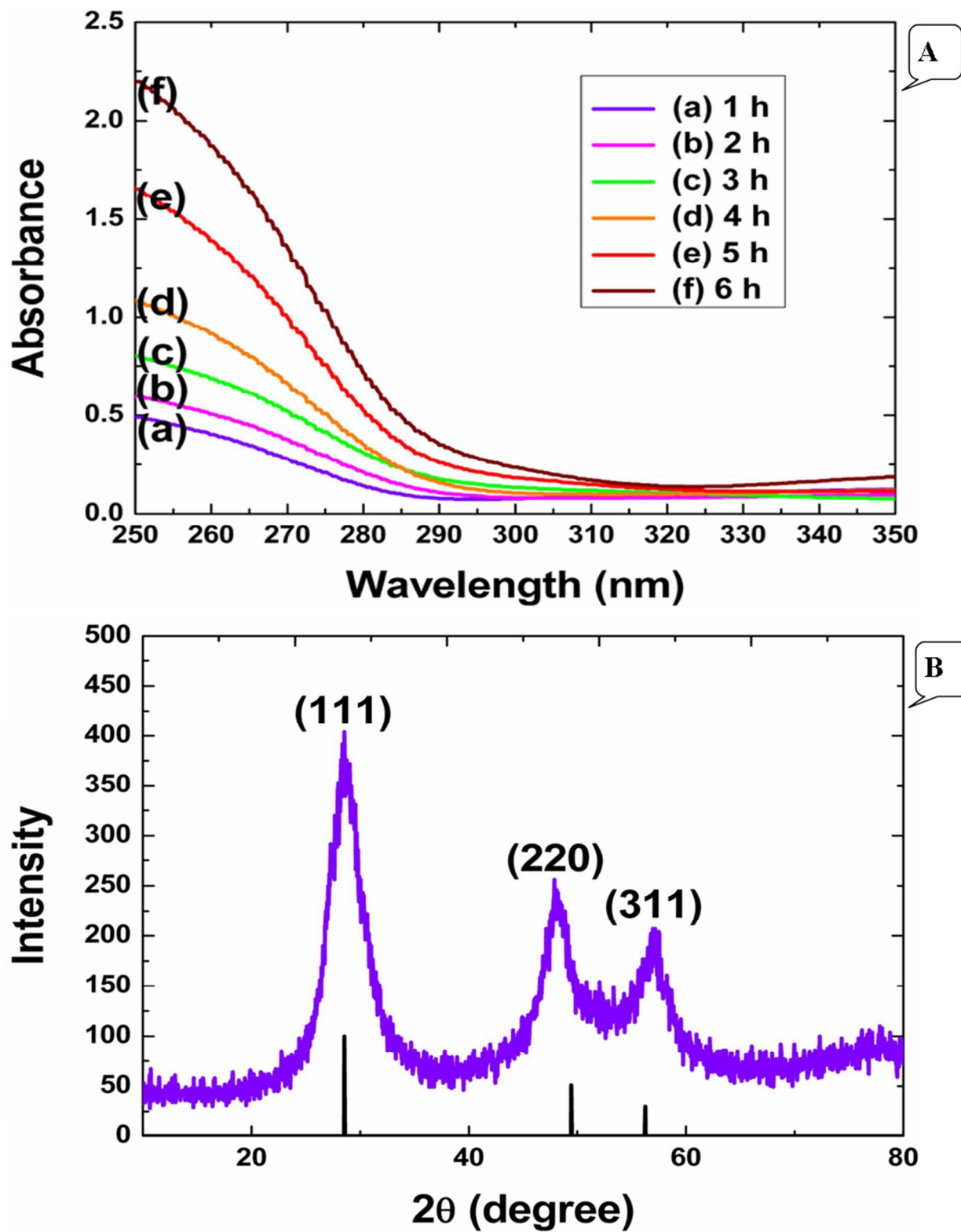


Fig. 2

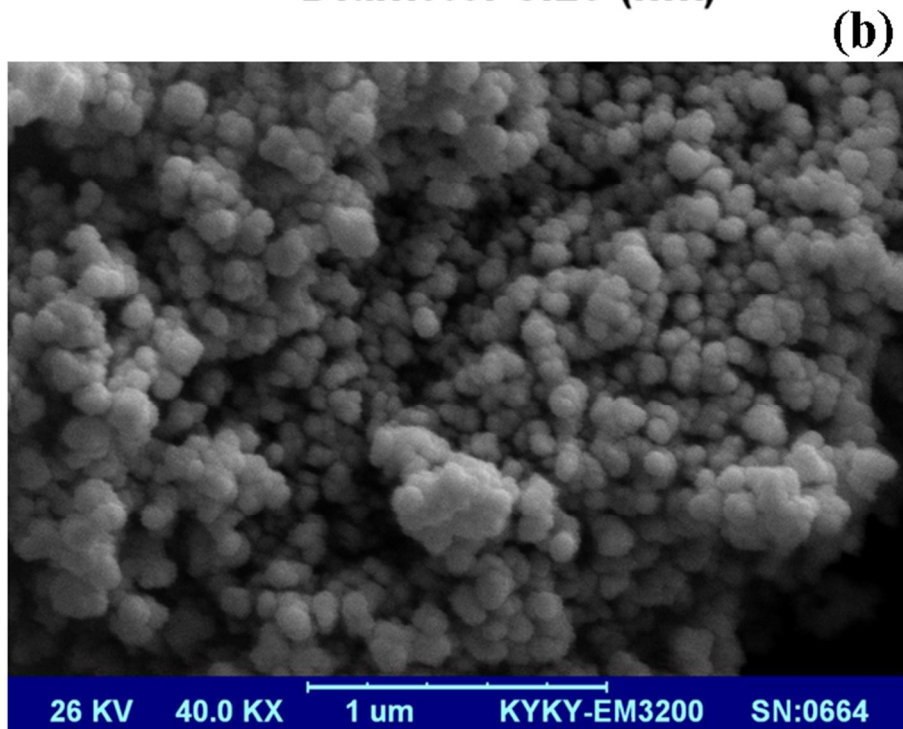
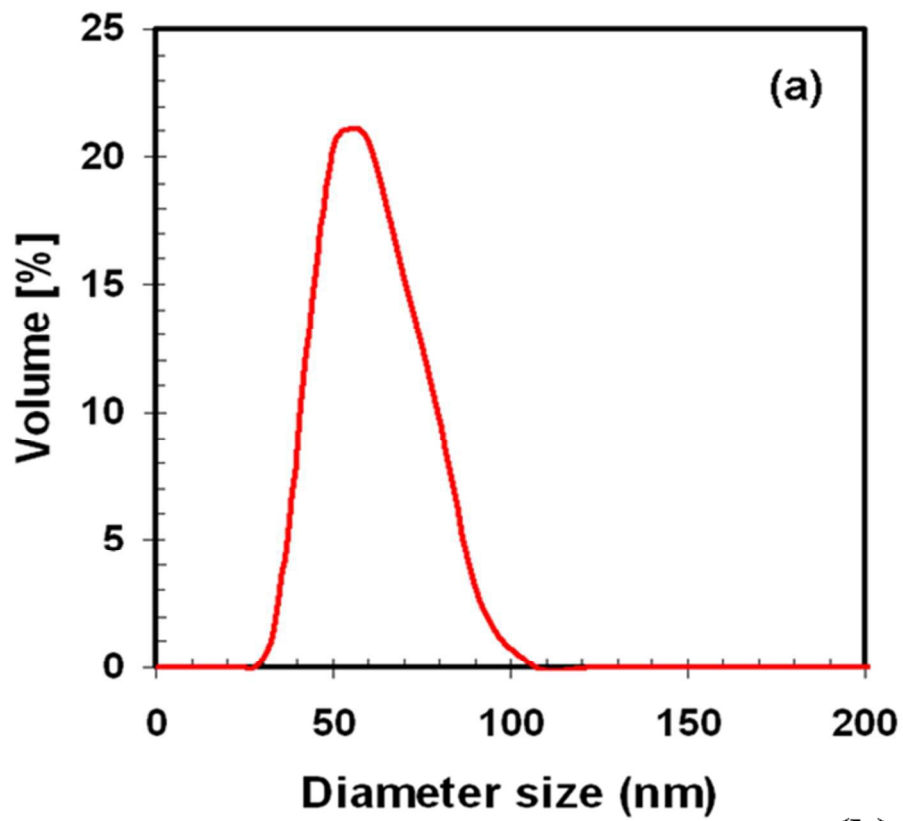


Fig. 3

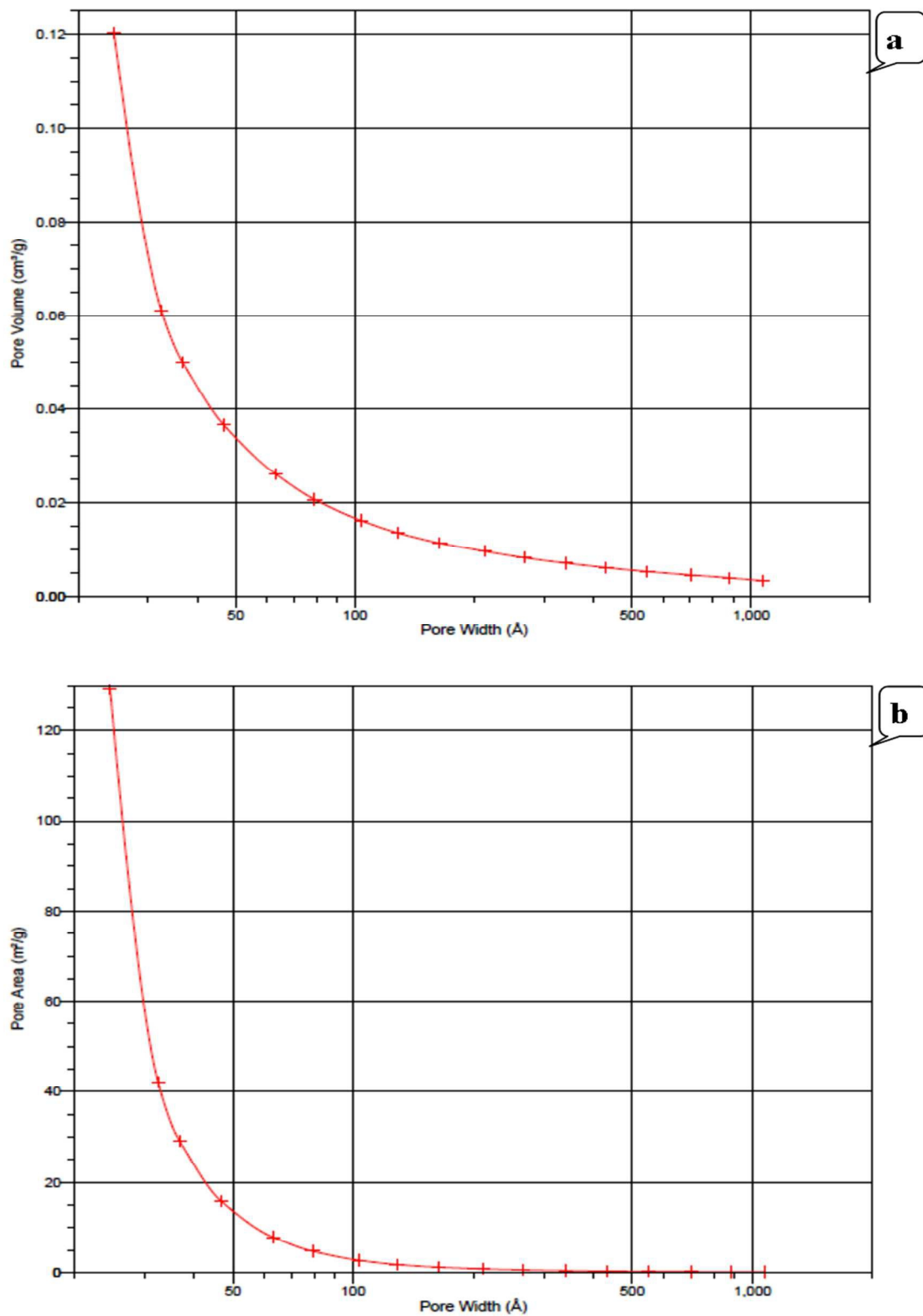


Fig. 4

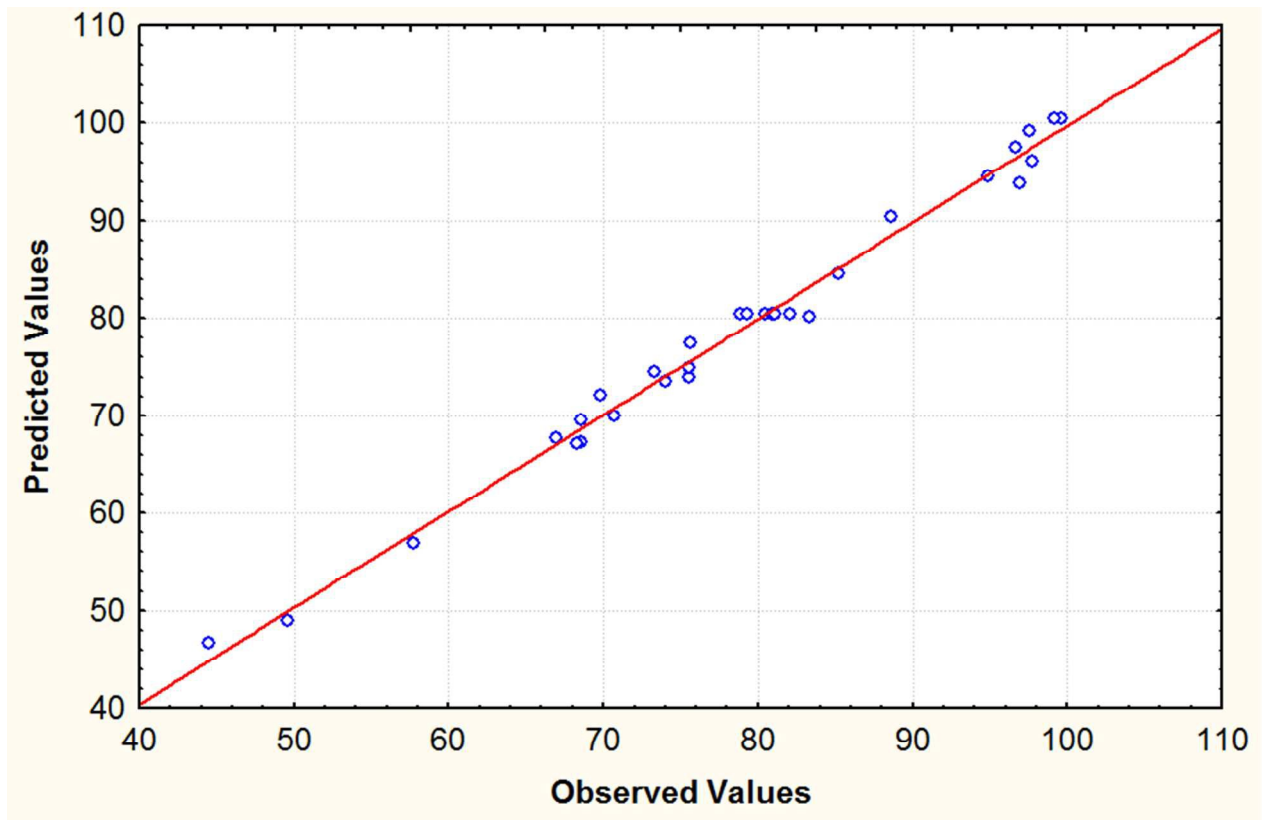


Fig. 5

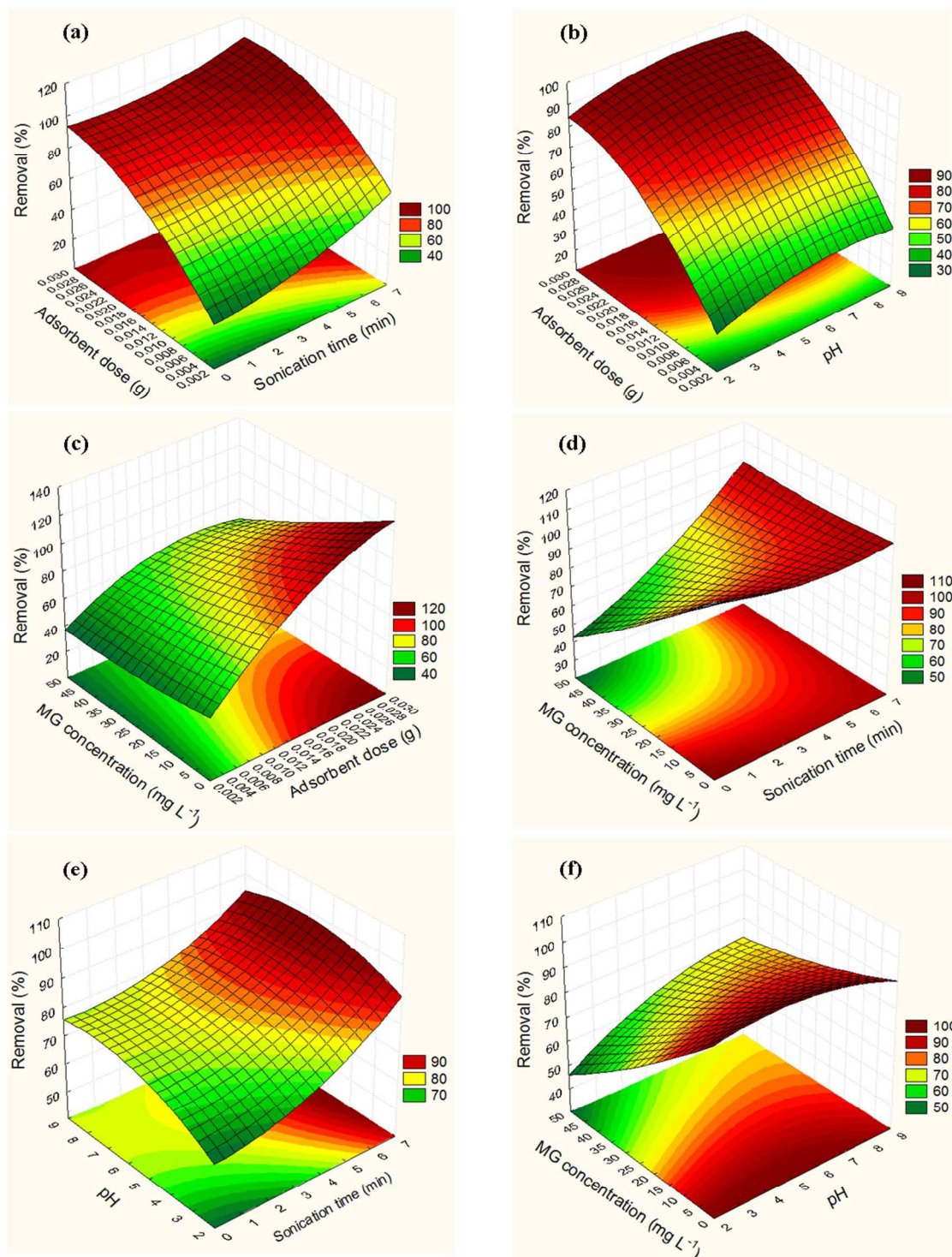


Fig. 6

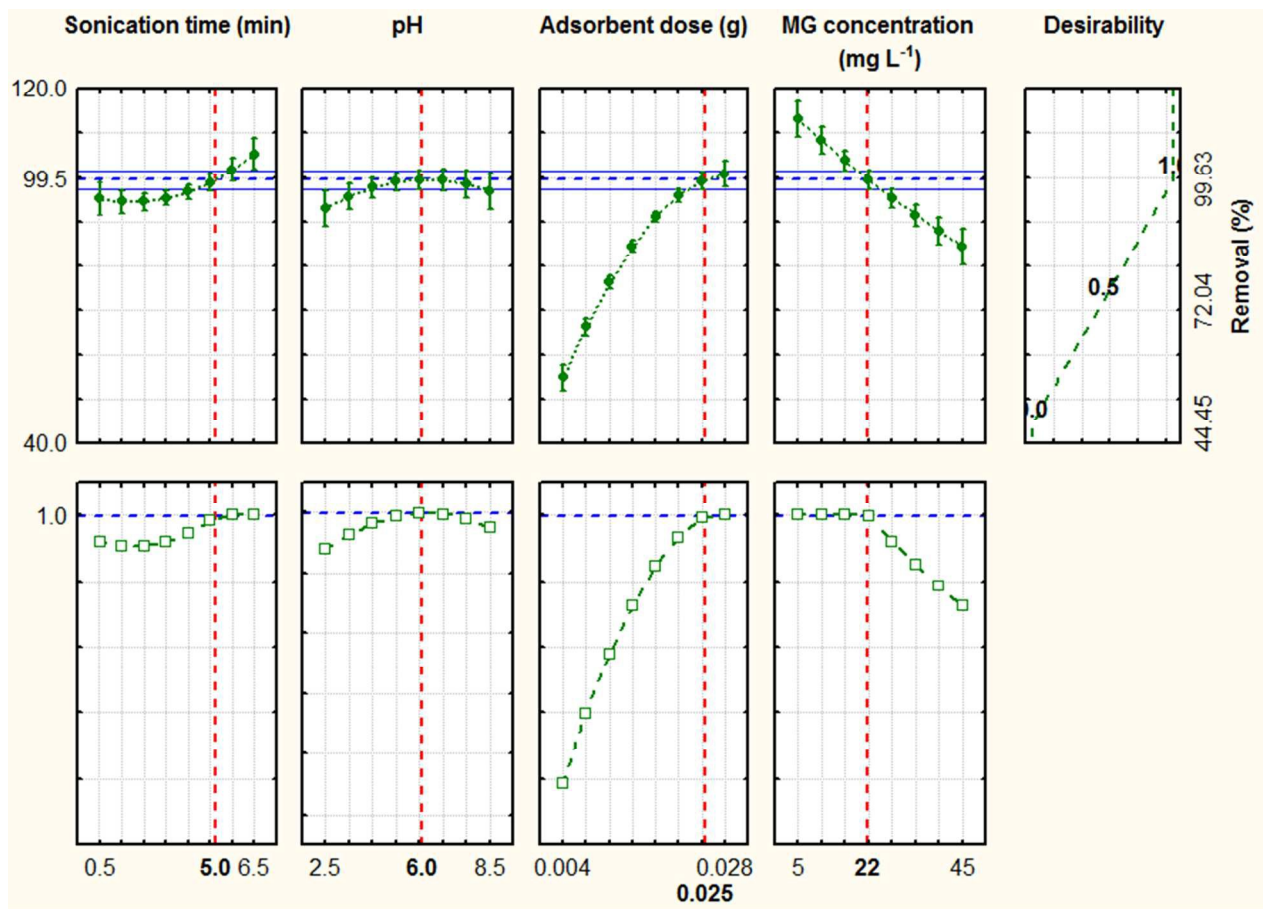


Fig. 7

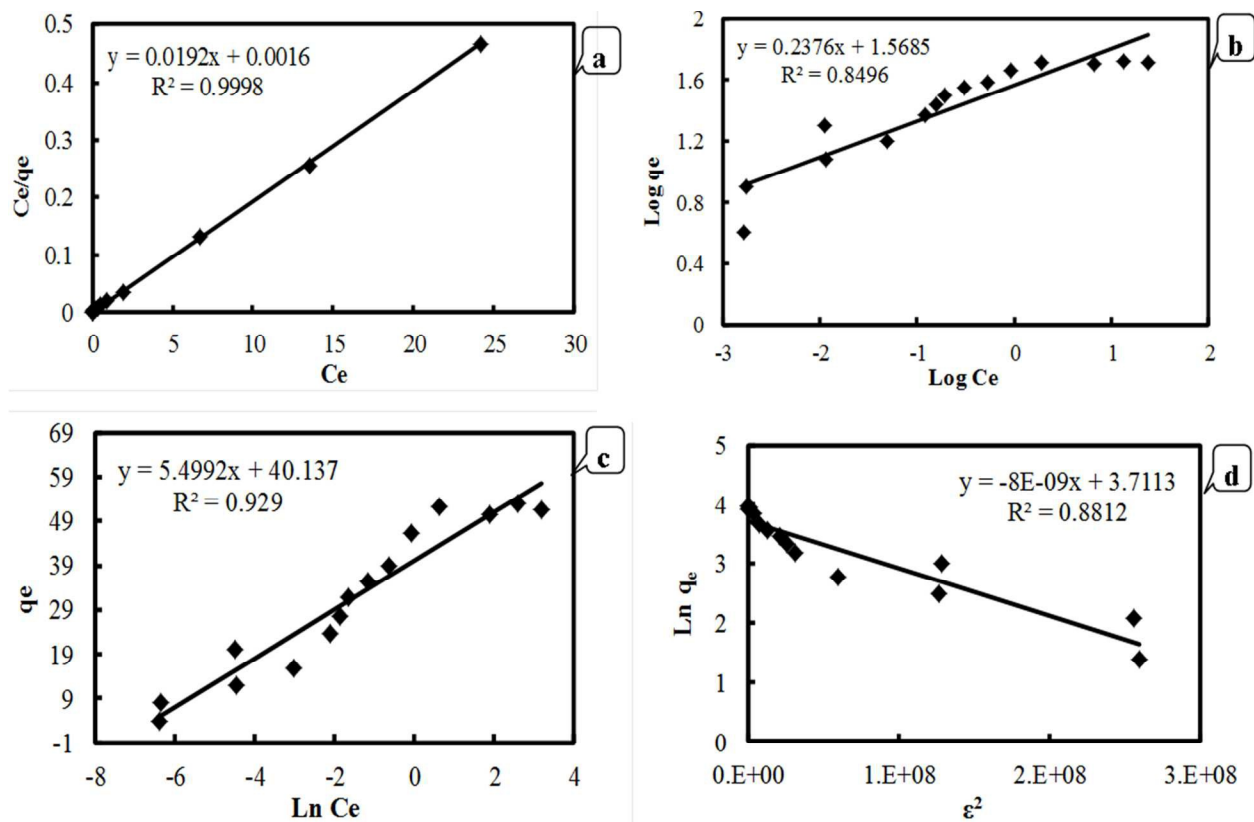


Fig. 8

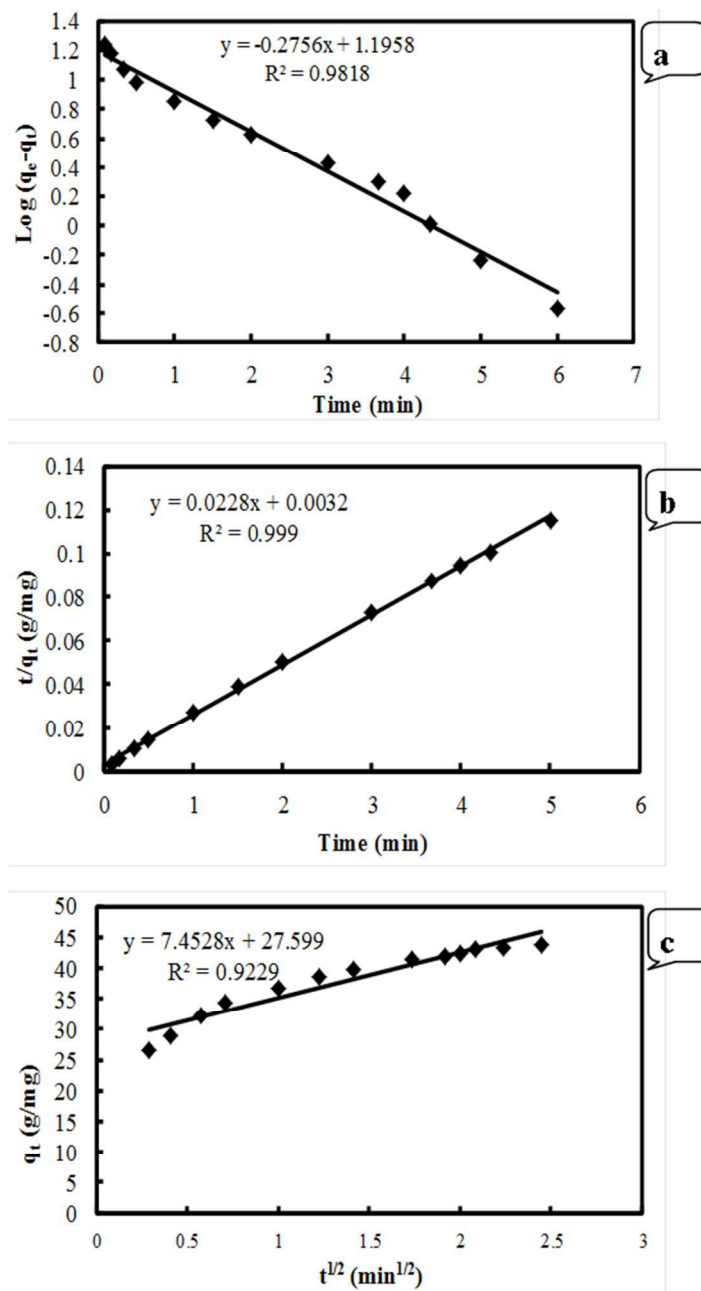


Fig. 9